

Soft Matter

Accepted Manuscript

This article can be cited before page numbers have been issued, to do this please use: N. P. Dhakal, M. Talwar, Z. Siddiquee, J. Karcz, P. Kula, P. Salamon and A. Jakli, *Soft Matter*, 2026, DOI: 10.1039/D6SM00284F.



This is an Accepted Manuscript, which has been through the Royal Society of Chemistry peer review process and has been accepted for publication.

Accepted Manuscripts are published online shortly after acceptance, before technical editing, formatting and proof reading. Using this free service, authors can make their results available to the community, in citable form, before we publish the edited article. We will replace this Accepted Manuscript with the edited and formatted Advance Article as soon as it is available.

You can find more information about Accepted Manuscripts in the [Information for Authors](#).

Please note that technical editing may introduce minor changes to the text and/or graphics, which may alter content. The journal's standard [Terms & Conditions](#) and the [Ethical guidelines](#) still apply. In no event shall the Royal Society of Chemistry be held responsible for any errors or omissions in this Accepted Manuscript or any consequences arising from the use of any information it contains.

Transient Negative Capacitance in Ferroelectric and Twist-Bend Ferroelectric Nematic Liquid Crystals

Netra Prasad Dhakal^{1,2}, Manisha Talwar^{1,3}, Zakaria Siddiquee^{1,3}, Jakub Karcz⁴, Przemysław Kula⁴, Peter Salamon⁵, Antal Jákli^{1,2,3*}

¹Advanced Materials and Liquid Crystal Institute, Kent State University, Kent, OH 44242, USA

²Materials Science Graduate Program, Kent State University, Kent, OH 44242, USA

³Department of Physics, Kent State University, Kent, OH 44242, USA

⁴Faculty of Advanced Technology and Chemistry, Military University of Technology, Warsaw, 00-908, Poland

⁵Institute for Solid State Physics and Optics, HUN-REN Wigner Research Centre for Physics, P.O. Box 49, Budapest H-1525, Hungary

*: Corresponding author: ajakli@kent.edu

Abstract:

The negative capacitance (NC) of ferroelectric materials can be used in conventional electronics to reduce the power dissipation. Recently, NC was shown (Phys. Rev. Appl., 24, 014029 (2025)) to exist in a fluid ferroelectric nematic (N_F) liquid crystal material as well.

Studies presented in this paper strongly indicate that NC exists in all ferroelectric nematic liquid crystal materials provided that the polarization switching time is larger than of the rise time of the applied square-wave voltage. Additionally, NC was studied in a recently discovered fluid twist-bend ferroelectric nematic liquid crystal (N_{TBF}) material while switching their ferroelectric polarization. In contrast to the 2 NC ranges found in conventional ferroelectric crystals and ferroelectric nematic liquid crystals, in the N_{TBF} phase the polarization switching happens in two steps leading to four negative capacitance ranges in the P-V hysteresis curves. Our measurements and analyses also provide estimates of the rotational viscosities and the physical mechanisms of the polarization switching steps in the N_{TBF} phase.

Keywords: Negative capacitance; Ferroelectric nematic liquid crystals, Twist-bend ferroelectric nematic liquid crystals; Power saving



I. Introduction

The capacitance (C) of a capacitor is given by $C = \frac{dQ}{dV}$ where Q is the charge stored on the electrodes and V is the voltage between them. The energy stored in a capacitor is $W = \frac{Q^2}{2C} = \frac{1}{2} QV$, which is positive for positive capacitance^{1,2}. In a ferroelectric material with a spontaneous polarization \vec{P}_s , the electric displacement \vec{D} that measures the free surface charge density on plates is $\vec{D} = \epsilon_0 \epsilon_r \vec{E}_F + \vec{P}_s$. Here $\epsilon_0 = 8.85 \cdot 10^{-12} \frac{C^2}{Nm^2}$ is the permittivity of vacuum, ϵ_r is the relative dielectric permittivity of the material and $\vec{E}_F = \vec{E} - \frac{\vec{P}_s}{\epsilon_0 \epsilon_r}$ is the electric field in the ferroelectric material. This provides that $\frac{\partial \vec{D}}{\partial \vec{E}_F} = \epsilon_0 \epsilon_r + \frac{\partial \vec{P}_s}{\partial \vec{E}_F} = \epsilon_0 \epsilon_r + \epsilon_0 \epsilon_F$, where ϵ_F is the ferroelectric permittivity. While ϵ_r is always positive, ϵ_F can be negative if $\frac{\partial \vec{P}_s}{\partial \vec{E}_F} < 0$. This was discussed by Landau and Khalatnikov already at the early days of ferroelectricity³. According to the Landau-Ginzburg theory, the polarization dependence of the free energy density of a ferroelectric material in an electric field $E_F = |\vec{E}_F|$ can be written as $f = aP_s^2 + bP_s^4 - E_F P_s$ ^{4,5}, where $a < 0$ and $b > 0$ are the Landau coefficients assuming second order paraelectric – ferroelectric phase transition. This corresponds to a double-well function with stable polarization values at the minima and an unstable $P_s = 0$, as depicted in Figure 1(a). Minimizing f with respect to P_s , we get for the electric field E_F inside the ferroelectric materials that $E_F = 2aP_s + 4bP_s^3$. The plot of P_s against E_F has an “S” shape (Figure 1(b)). In this curve the orange shaded thermodynamically unstable range represents $\epsilon_F < 0$ where the polarization changes opposite to the electric field, therefore the capacitance becomes negative.⁶ In this range, E_F decreases while the average P_s is increasing (switching from negative to positive direction), i.e., while the capacitor is charging^{6,7}.

In addition to solid ferroelectric⁸⁻¹⁰ and antiferroelectric^{11,12} materials, transient negative capacitance (NC) has also been reported recently in several 3D fluid ferroelectric nematic liquid crystals (N_F)¹³. N_F liquid crystals consist of highly polar molecules with dipole moments greater than $9D$. When cooled from paraelectric nematic phase (N) characterized by an averaged molecular direction ($\hat{n} = -\hat{n}$) (see Figure 2(a)) to the ferroelectric nematic phase, these dipoles align along a particular direction breaking the inversion symmetry of the director ($\hat{n} \neq -\hat{n}$) and



show spontaneous polarizations in the order of $P_s \sim 5 - 8 \mu\text{C}/\text{cm}^{214-17}$ (see Figure 2(b)). In contrast to solid ferroelectrics where the polarization is switching via boundary motion, in fluid ferroelectric LC the polarization can rotate with respect to an axis normal to the electric field.^{18,19} When a square wave electric field is applied through a series resistance R (Figure 1(c)), the polarization flips following the direction of the applied voltage as illustrated in Figure 1(d)^{13,20-24}. To observe NC, i.e., a negative slope of the voltage dropping on the ferroelectric fluid, P_s should rotate after the applied voltage has fully switched. The viscosity of N_F material and therefore the switching time highly depends on the temperature^{25,26}.

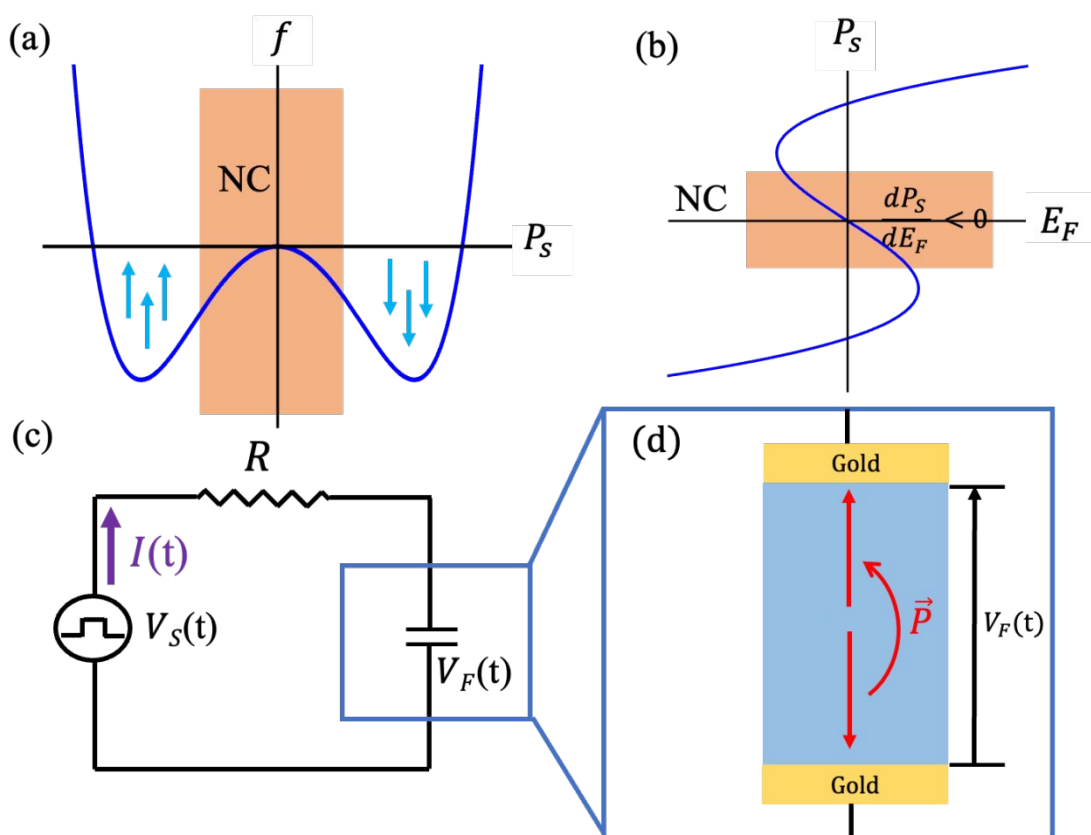


Figure 1: Illustration of the principle and experimental realization of ferroelectric materials with transient negative capacitance. (a): Schematic free energy density f as a function of the ferroelectric polarization P_s of a ferroelectric material with second order paraelectric-ferroelectric phase transition. (b): Ferroelectric polarization P_s as a function of the electric field in a ferroelectric material with $f(P_s)$ corresponding to (a). Orange shaded areas indicate unstable state. (c): Schematic representation of a measuring circuit consisting of an external voltage source V_s , a resistance R connected in series with a ferroelectric capacitor. (d): Illustration of flipping of the polarization upon applying square wave voltage $V_s(t)$ of the ferroelectric liquid crystal sandwiched between gold electrodes.



Previous experiments carried out in the geometry shown in Figure 1(d) on several N_F materials, found evidence for transient NC only in a room temperature N_F mixture with a relatively high rotational viscosity ($\gamma \approx 20 \text{ Pa} \cdot \text{s}$) and failed to demonstrate it on the two high temperature prototypical N_F substances RM734²⁷ and DIO¹⁶ with much smaller rotational viscosity values.

In this paper, we present redesigned studies on the low viscosity prototypical N_F materials and on a material having both N_F phase and a ferroelectric twist bend nematic N_{TBF} phase^{28–31}. The formation of the N_{TBF} phase is due to the competition between bend elasticity, molecular shape anisotropy, and polar interactions, resulting in a chiral symmetry breaking^{28,32}. The vector of local spontaneous polarization follows an oblique helicoidal trajectory around a polar twist bend axis making a conical tilt angle θ (see Figure 2(c)) which is similar to the previously reported dielectric twist bend nematic phase (N_{TB})^{33,34}. Note that while the local polarization rotates around the helical axis, its component perpendicular to the helical axis is averaged out over one pitch, resulting in a decreased bulk polarization parallel to the helical axis. The pitch of the N_{TBF} phase is in the range from a few hundred nano meters^{28,35} to a few micrometers³⁶. When an electric field is applied in N_{TBF} , the polarizations rotate towards the electric field, the cone angle decreases to allow the polarization to completely align along the field.^{28,37}

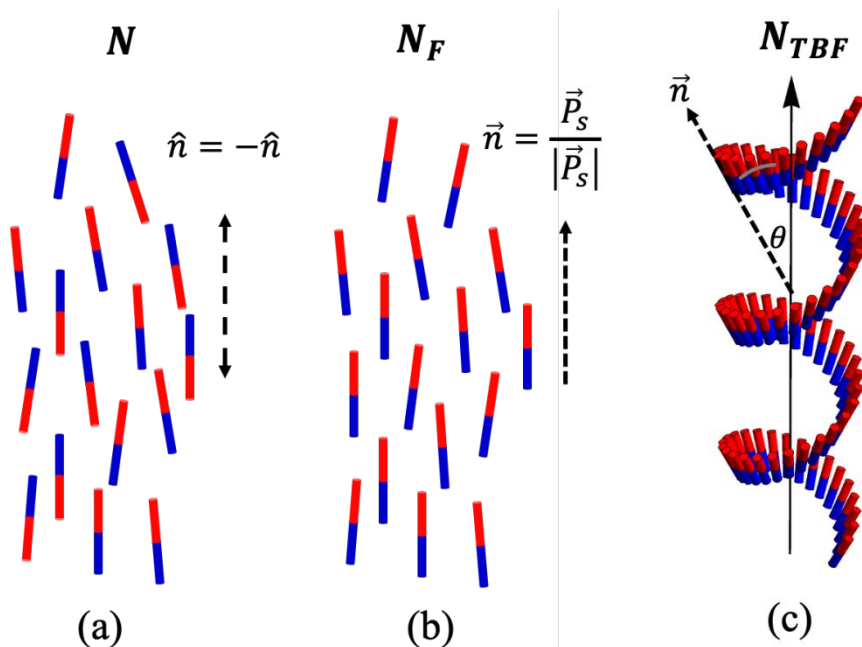


Figure 2: Schematic illustration of nematic (N), ferroelectric nematic (N_F) and twist bend ferroelectric nematic (N_{TBF}) liquid crystal phases. Red (blue) parts indicate positively (negatively) charged areas forming molecular dipoles. (a): N phase where equal number of dipoles are pointing up and; (b): N_F phase, where most molecular dipoles point in the same direction leading



to a spontaneous polarization \vec{P}_s along the director \vec{n} ; (c): N_{TBF} phase where the director rotates around the helicoidal axis making an angle (θ) with the local polarization direction.

We will find strong evidence that NC is inherent property of N_F materials, and it can be detected in all N_F (and any ferroelectric) materials provided that the rise time of the applied voltage V_S is smaller than the switching time of the polarization. We will also show that NC can be detected even in the N_{TBF} phase, but instead of a single negative peak in the V_F , there are double negative peaks. We will argue that this is due to the two-step polarization process related to the inversion of the helicoidal axis and the field-induced decrease of the cone angle.

II. Materials and Methods

Three compounds showing ferroelectric nematic phase have been studied. The two prototypical compounds, 4-[(4-nitrophenoxy)carbonyl] phenyl 2,4-dimethoxybenzoate (RM734)²⁷, and 2,3',4',5'-tetrafluoro[1,1'-biphenyl]-4-yl 2,6-difluoro-4-(5-propyl-1,3-dioxan-2-yl) benzoate (DIO)³⁸ with molecular structures and phase transition temperatures shown in Figure 3(a) and Figure 3(b). The substance is 4'-(difluoro(3,4,5-trifluorophenoxy)methyl)-2,3',5'-trifluoro-[1,1'-biphenyl]-4-yl 2,6-difluoro-4-(5-propyl-1,3-dioxan-2-yl)benzoate (JK 103) with chemical structure and phase transition temperatures shown in Figure 3(c). In addition to the N_F phase, JK103 also has a twist-bend ferroelectric N_{TBF} phase.²⁸

All three materials are filled inside 20 μm cells by capillary action between gold patterned electrodes with 0.4 mm \times 0.4 mm areas, as shown in Figure 3(d, e). 100 Hz square wave voltages V_S generated using an Agilent 33120A function generator were applied between the gold electrodes. The time dependence of V_S is monitored on Channel 1 of a Keysight 3024A oscilloscope. The liquid crystal (LC) cell is connected in series with a resistor R , and the voltage drop across the LC cell, V_F , is measured on Channel 2 of the same oscilloscope. The role of the series resistor R is to adjust the charging of the capacitor by switching the ferroelectric polarization with time $\tau = RC$ of the liquid crystal cell (see Figure 5c). To observe negative capacitance, it is important to have larger polarization switching time than the rise time of the voltage, which necessitates the use of square wave voltage. Identical cables are used for both channels, and the cable lengths are kept as short as possible to minimize parasitic effects.



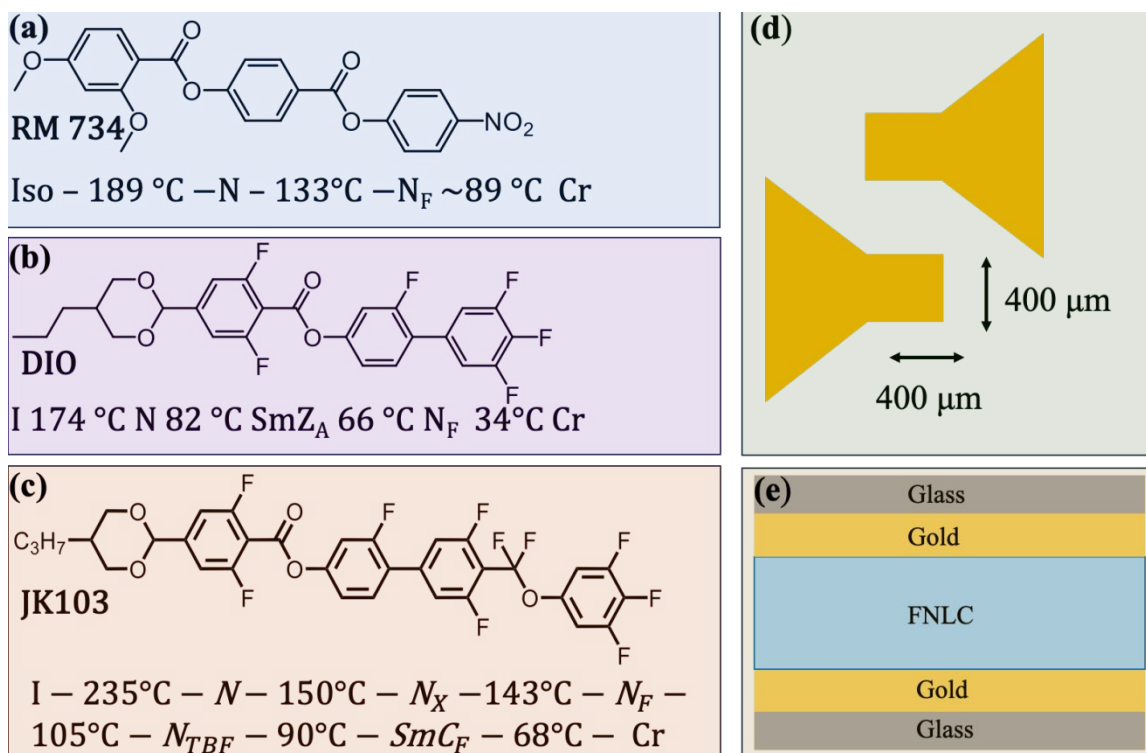


Figure 3: Materials and methods (a-c): Chemical structures and phase transition temperatures of the studied materials RM734, DIO and JK 103, respectively; (d): Patterns of gold electrode on glass substrates overlapping on 0.4 mm × 0.4 mm area; (e): Schematic cross section of the cell where the ferroelectric materials are sandwiched between gold electrodes covering the glass substrates.

III. Experimental Results

Time dependences of the rectangular source voltage (V_S) and the ferroelectric voltage (V_F), measured using a circuit shown in Figure 1(c) are seen for RM734 and DIO for various resistances in Figure 4(a) and Figure 5(a), respectively. After quickly switching V_S between ± 2.5 V and ± 1.5 V, V_F first changes sign, then reverses within 0.2 ms and ≈ 50 μs, then bounces back and saturates in about 2 ms and 0.5 ms for RM734 and DIO, respectively. Such a behavior is typical for ferroelectric⁸⁻¹⁰ and antiferroelectric^{11,12} crystals and was also found for a room temperature N_F ¹³ LC. Since the rotational viscosity of nematic LCs increase upon cooling, for both RM734 and DIO, the switching times increase with decreasing temperatures (see Figure 4(b) and Figure 5(b)). The switching times determined by the peak positions in V_F are plotted in Figure 4(c) and Figure 5(c) with respect to the resistance R connected in series with the LC cells for RM734 and DIO, respectively. For both materials the switching time is a linear function of R and the fitted lines intercept the x-axis at $R_i \approx -8$ kΩ and at $R_i \approx -12$ kΩ for RM734 and DIO, respectively.



These values are close to that obtained on a room temperature N_F mixture¹³ and the absolute values of R_i correspond to the resistance of the liquid crystal film ($|R_i| = R_{LC}$). In the entire N_F range of RM734 and DIO the ohmic leakage current I_Ω is less than 5% of the ferroelectric polarization current as can be seen in Figure 4a and Figure 5a. Taking this into account, the ferroelectric polarization was calculated as $P(t) \approx \frac{\int (V_S(t) - V_F(t)) dt}{RA} - \frac{\int I_C dt}{A} - \int I_\Omega dt$. The polarization as a function of voltage V_F are plotted in Figure 4(d) and Figure 5(d) for RM734 and DIO, respectively. Negative slopes indicated by magenta ellipses correspond to ranges with negative capacitance (NC). The saturated value of polarization for RM734 at 120 °C is $P_s \approx 0.055 \frac{C}{m^2}$ and for DIO at 50 °C is $P \approx 0.04 \frac{C}{m^2}$ in agreement with literature values.^{38,39}

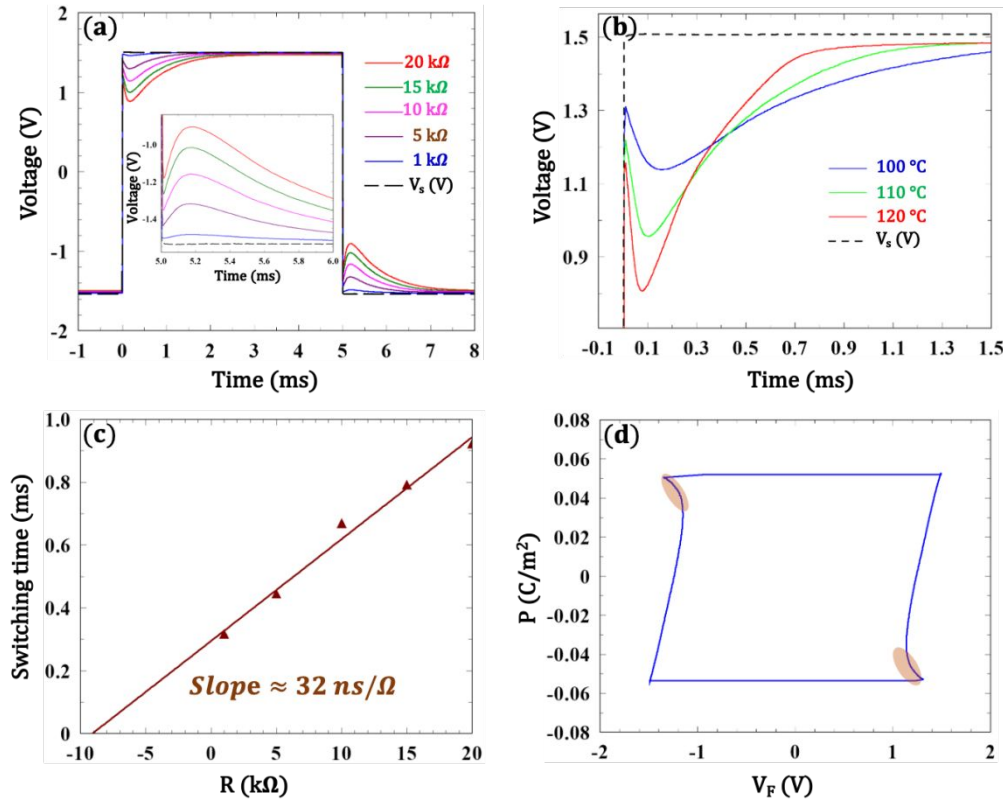


Figure 4: Summary of the measurement results obtained on a 20 μm RM734 cell. (a): Time dependences of the rectangular source voltage (V_S) and the voltage dropping on the ferroelectric nematic liquid crystal film (V_F) for various resistance at 100 °C; (b): Time dependence of V_S and V_F for resistance $R = 10 \text{ k}\Omega$ at selected temperatures; (c): Switching time with respect to R indicating linear behavior with slope $\approx 32 \frac{\text{ns}}{\Omega}$ and intercept of the zero switching time at $R_i \approx -8 \text{ k}\Omega$; (d): Polarization as a function of voltage V_F dropping on the ferroelectric LC film at 120 °C. Negative slopes indicated by magenta shapes correspond to ranges with negative capacitance (NC).



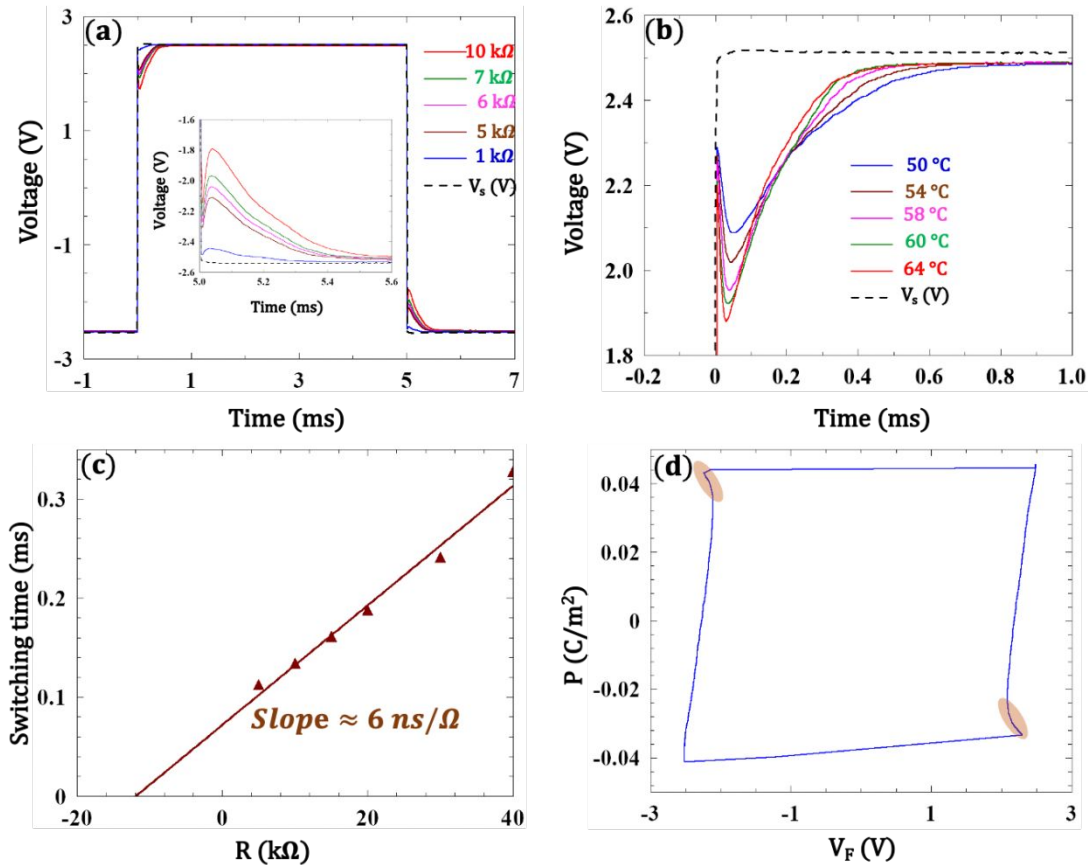


Figure 5: Summary of the experimental results obtained on a 20 μm DIO cell. (a): Time dependences of the rectangular source voltage (V_S) and the voltage dropping on the ferroelectric nematic liquid crystal film (V_F) for various resistance at 60 °C; (b): Time dependence of V_S and V_F for resistance $R = 7 \text{ k}\Omega$ at selected temperatures; (c): Switching time with respect to R indicating linear behavior with slope $\approx 32 \frac{\text{ns}}{\Omega}$ and intercept of the zero switching time at $R_i \approx -12 \text{ k}\Omega$; (d): Polarization as a function of voltage V_F dropping on the ferroelectric LC film at 50 °C. Negative slopes indicated by magenta shapes correspond to ranges with negative capacitance (NC).

Summary of the results obtained on 20 μm JK103 films in the N_F and N_{TBF} phases are shown in Figure 6. Figure 6(a) and Figure 6(b) show the time dependences of V_F at various resistance values connected in series with the LC cell in comparison with the square wave source voltage of $V_S = 2.2 \text{ V}$ at 110 °C in the N_F phase and at 100 °C in the N_{TBF} phase, respectively. Our polarized optical microscopy observations revealed that at this source voltage the sample goes to homeotropic indicating full polarization switching. Similar to the observations in RM734 and DIO, in the N_F phase V_F is decreasing (increasing) while V_S is increasing (decreasing) within 0.1 ms after the sign inversion of V_S , then bounces back and reaches equilibrium value within 1 ms. In



contrast to that found in the N_F phase, in the N_{TBF} phase the equilibrium is reached in two steps showing two peaks of $V_F(t)$ as shown in Figure 6(b) at 100 °C.

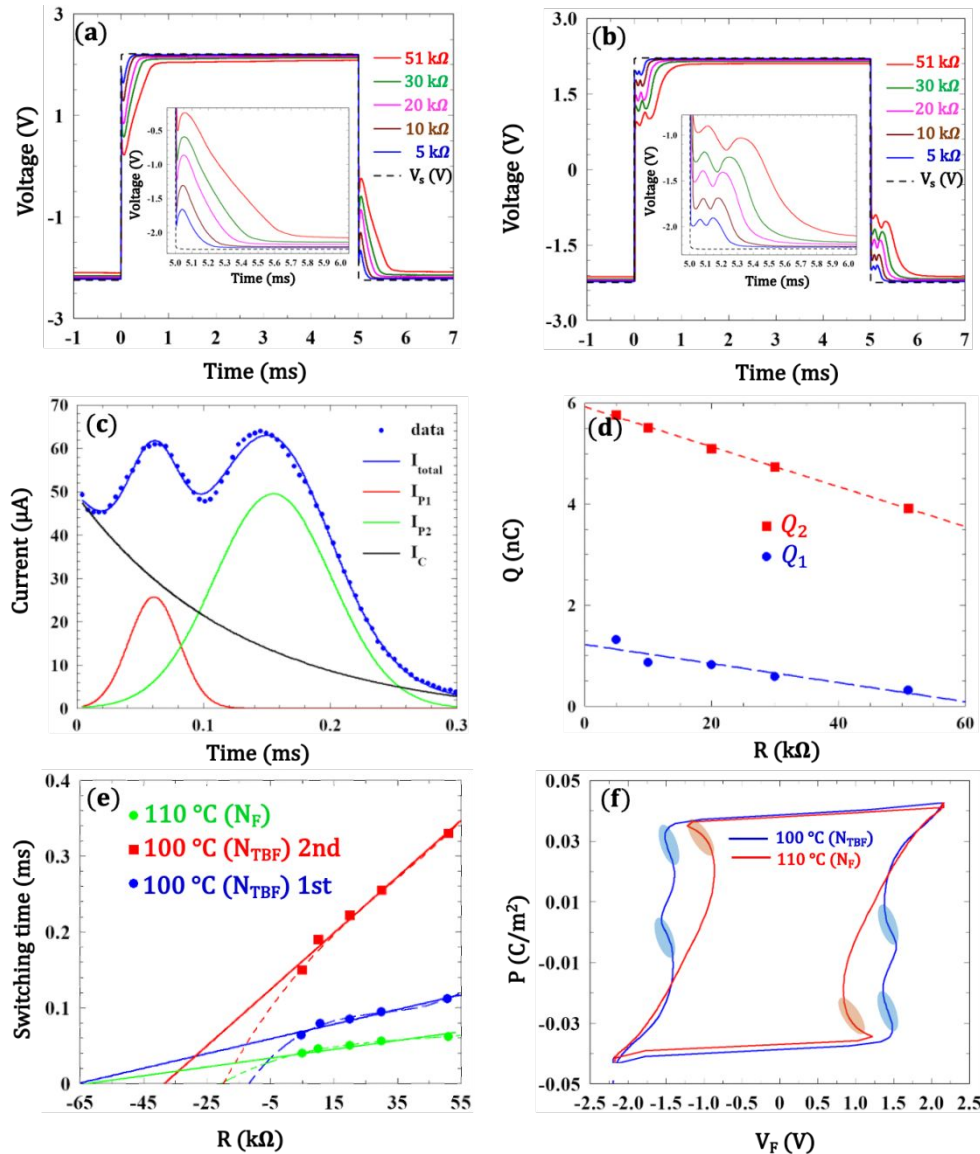


Figure 6: Summary of the results obtained on a 20 μm JK103 cell. (a): Time dependences of the rectangular source voltage (V_s) and the voltage dropping on the ferroelectric nematic liquid crystal film (V_F) for various resistances in the N_F phase at 110 °C; (b) Time dependences of the rectangular source voltage (V_s) and the voltage dropping on the ferroelectric nematic liquid crystal film (V_F) for various resistance in the N_{TBF} phase at 100 °C; (c) Time dependence of the current for $R = 5$ kΩ; (d) Polarization charges Q_1 and Q_2 under peak 1 and peak 2 in (c) as a function of resistance applied in series with the LC cell. (e) Switching times (defined as the time positions of the fitted current peaks in (c)) with respect to R at 110 °C (green dots) and at 100 °C related to the first peak (blue dots) and for the 2nd peak (red squares). Linear fits intercept the horizontal axis at $R_i \approx -64, 62$ and 38 kΩ for the green, blue and red data points respectively. (f): $P - V_F$ plots in the N_F and N_{TBF} phases. Magenta (light blue) ellipses show NC ranges in the N_F phase and N_{TBF} phase, respectively.



The current going through the sample can be calculated as $I(t) = (V_S(t) - V_F(t))/R$. At $R = 5 \text{ k}\Omega$ $I(t)$ is shown in Figure 6(c). The area $\int I_C dt$ below the capacitive decay current I_C corresponds to the capacitive charge $Q_C = C \cdot V_F = \epsilon_o \epsilon_r \frac{A}{L} \cdot V_F$ and can be estimated as $Q_C \sim \frac{5 \cdot 10^{-5} \text{ A} \times 2 \cdot 10^{-4} \text{ s}}{2} \sim 5 \text{ nC}$. With $V_F \sim 2.5 \text{ V}$, $L = 20 \text{ }\mu\text{m}$ and $A = 0.16 \text{ mm}^2$ it provides $\epsilon_r (\sim 100 \text{ Hz}) \approx 2.5 \cdot 10^4$. As argued by Clark et al²³ and verified experimentally²⁴ such a high value is related to the capacitance of the insulating layer that for conducting surfaces, such as the gold in our case, is the thickness ($L_i \sim 1 \text{ nm}$) of the anchored FNLC molecules. We note that for $L \approx 3 \text{ }\mu\text{m}$ film with bare ITO layers $\epsilon_r (\sim 100 \text{ Hz}) \approx 4 \cdot 10^3$ was measured in²⁸. Assuming similar $L_i \sim 1 \text{ nm}$ for gold and ITO surfaces and taking into account that in our case $L \approx 20 \text{ }\mu\text{m}$, the ratio of the apparent dielectric constant measured by Karcz et al and estimated by us is $\frac{25}{4} \approx 6.5 \approx \frac{20}{3} = 6.7$. Polarization charges Q_1 and Q_2 under peak 1 and peak 2 in (c) as a function of resistance applied in series with the LC cell are plotted in Figure 6(d). Both Q_1 and Q_2 linearly decreasing with the resistance R .

The switching times defined as the time positions of peak 1 and peak 2 (see Figure 6(c)) as a function of R are shown in the N_F phase at $110 \text{ }^\circ\text{C}$ and at $100 \text{ }^\circ\text{C}$ in the N_{TBF} phase (representing peak 1 and peak 2) in Figure 6(e). The fastest switching with the least R dependence was found in the N_F phase (green data points in Figure 6(e)). The switching time related to the first peak in N_{TBF} is about 40% larger at $100 \text{ }^\circ\text{C}$ than at $110 \text{ }^\circ\text{C}$ (blue data points in Figure 6(e)). The switching time related to the 2nd peak in the N_{TBF} phase (red data points in Figure 6(e)) is three times larger and it shows the strongest R dependence. Fitting the R -dependences by linear functions as for RM734 and DIO, the resistances at zero switching times can be approximated as $R_i \approx -64, -62$ and $-38 \text{ k}\Omega$ for the green, blue and red data points respectively. These values are much larger than the $R_i \approx -10 \Omega$ found for RM734 and DIO. We note that in this case, the best fits are not the linear functions, but those that intercept the x axis at $R_i \approx -20, -12$ and $-20 \text{ k}\Omega$ for $110 \text{ }^\circ\text{C}$ in N_F , 1st and 2nd peak at $100 \text{ }^\circ\text{C}$ in the N_{TBF} phase, respectively.

Finally, Figure 6(f) compares the $P - V_F$ plots in the N_F and N_{TBF} phases, where $P = Q_P / A = (\int I_P dt) / A$. In both phases the saturated polarization is $P_s \approx 0.04 \frac{\text{C}}{\text{m}^2}$ in agreement with reference²⁸. Additionally, while similar to that found for RM734 and DIO, there are two ranges (highlighted by magenta ellipses) showing NC in the N_F phase, in the N_{TBF} phase there are 4 NC



regions (highlighted by light blue ellipses). This is related to the double peaks seen in the N_{TBF} phase.

IV. Discussion

In previous results¹³ the transient capacitance (NC) could be shown in sandwich cells only for a room temperature N_{F} mixture with switching times around 1 ms under $5 \frac{V}{\mu\text{m}}$ fields. Here we showed similar NC also for the two prototypical N_{F} materials RM734 and DIO. Additionally (not discussed here), we have verified the presence of NC for all other (~half a dozen) N_{F} materials we have studied. This strongly indicates that all ferroelectric nematic liquid crystal (FNLC) materials have NC behavior. As it was argued previously, the necessary condition for the transient NC behavior is that the switching of the ferroelectric polarization be delayed compared to the rise time τ_r of the applied voltage V_s . The switching time of the polarization can be given as $\tau \approx \frac{\pi L \gamma}{P V_F}$ ²³, where L is the film thickness, γ is the rotational viscosity of the material, and V_F is the voltage drop on the N_{F} LC. In previous measurements the rise time was $\tau_r \approx 0.2$ ms, the film thickness was $L = 4$ μm and $V_F \leq 20$ V. This means that the rotational viscosity of the material had to be $\gamma \geq \frac{\tau_r P V_F}{\pi L} \approx 10$ Pa · s. This was true only for the previously observed room temperature mixture KPA02 where $\gamma \approx 20$ Pa · s, explaining why we could detect only for that N_{F} LC material. In our present setup $\tau_r \approx 1$ μs and $L = 20$ μm , thus allowing us to measure NC in N_{F} LCs with $\gamma \geq 2$ mPa · s. The rotational viscosities of the studied FNLC compounds can be calculated from the intercepts R_i of the linear fits of the $\tau(R)$ functions as shown for RM734 and DIO in Figure 4(c) and Figure 5(c), respectively. Since $|R_i| = R_{\text{LC}} = \frac{L \gamma}{A P^2}$ ¹³, from $R_{\text{LC}} = 8$ k Ω for RM734 with $P_s \approx 6$ $\mu \frac{\text{C}}{\text{cm}^2}$ and $R_{\text{LC}} = 12$ k Ω for DIO with $P_s \approx 4.5$ $\mu \frac{\text{C}}{\text{cm}^2}$, we get that $\gamma \approx 0.23$ Pa · s for RM734 at 100 °C, and $\gamma \approx 0.21$ Pa · s for DIO at 60 °C. These values are indeed measurable by our method and are reasonable.

In addition to verifying the required experimental conditions to measure NC in FNLCs, the other significant result of our work is the observation of the double current peak in the N_{TBF} phase of JK103. This is in contrast to previous polarization measurements where only single polarization current peaks were observed in the N_{TBF} ^{28,31,37} of the same JK103 phase and in the so called $^{\text{HC}}N_{\text{F}}$ ³². We note, however, that indication of double polarization peaks was observed in the tilted helical



smectic SmC_P^H phase of JK103³⁷ and in the N_{TBF} and HEC phases of another ferroelectric nematic substances.^{32,40} The peak forming at decreasing fields was assigned to the increase of the heliconical angle θ from zero to the equilibrium value θ_o , whereas the peak appears in increasing fields was assigned to the polarization flipping between $-P_s \cos\theta_o$ and $+P_s \cos\theta_o$ values.

In our measurements we have observed the two peaks under rectangular fields, thus we distinguish them by the switching times and not by the switching voltages. To find out the underlying physical mechanisms of these peaks, in addition to the positions of the fitted Gaussian peaks seen in Figure 6(c), we also measured the areas representing the polarization charges Q_1 and Q_2 under these peaks, as shown in Figure 6(d). The R dependence of both Q_1 and Q_2 decrease with R , and their sum is decreasing from $Q_1 + Q_2 \approx 7 \text{ nC}$ at $5 \text{ k}\Omega$ to $Q_1 + Q_2 \approx 4.2 \text{ nC}$ at $51 \text{ k}\Omega$. This is likely because V_F is decreasing at increasing R , i.e., that less voltage will drop on the sample. Figure 6(a) shows that when $R = 51 \text{ k}\Omega$, V_F decreases from 2.2 V to 2.05 V at 110°C in the N_F phase and to 2.1 V at 100°C in the N_{TBF} phase. In fact, taking into account these values and the geometry of the films ($L = 20 \mu\text{m}$ and $A = 0.16 \text{ mm}^2$), we get for the DC conductivity values that $\sigma_{DC} = 1.8 \times 10^{-9} (\Omega\text{m})^{-1}$ at 110°C and $\sigma_{DC} = 1.3 \times 10^{-9} (\Omega\text{m})^{-1}$ at 100°C . As $V_s = 2.2 \text{ V}$ was chosen that it was just slightly above the full polarization switching value when no resistance was connected in series to the LC film, even small decrease of V_F when a resistance is in series leads to incomplete polarization switching. This may also explain the R dependences of the ratios of peak areas Q_2/Q_1 that is increasing from 4.4 at $R = 5 \text{ k}\Omega$ from to 12.6 at $R = 51 \text{ k}\Omega$. The variation of the charge involved in the flipping of the polarization between $-P_s \cos\theta_o$ and $+P_s \cos\theta_o$ is $Q_f = 2P_s \cos\theta_o$, while the one involved in the change of the cone angle from θ_o to 0 is $Q_\theta = 2P_s(1 - \cos\theta_o)$. Assuming that the cone angle is smaller than 45° , we conclude that $Q_f = Q_2$ and $Q_\theta = Q_1$. Schematic representation of the polarization switching mechanisms involving variation of the cone angle ($\theta - mode$) and flipping of the polarization ($P - flip$) and leading to two current peaks shown in Figure 7. This is in accordance with the model by Gibb et al.⁴¹ Note that polarization rotations corresponding to the increase and decrease of the tilt result only one peak characterized with one switching time. The second peak, corresponding to the polarization flip, has a different switching time, thus that appears separately.



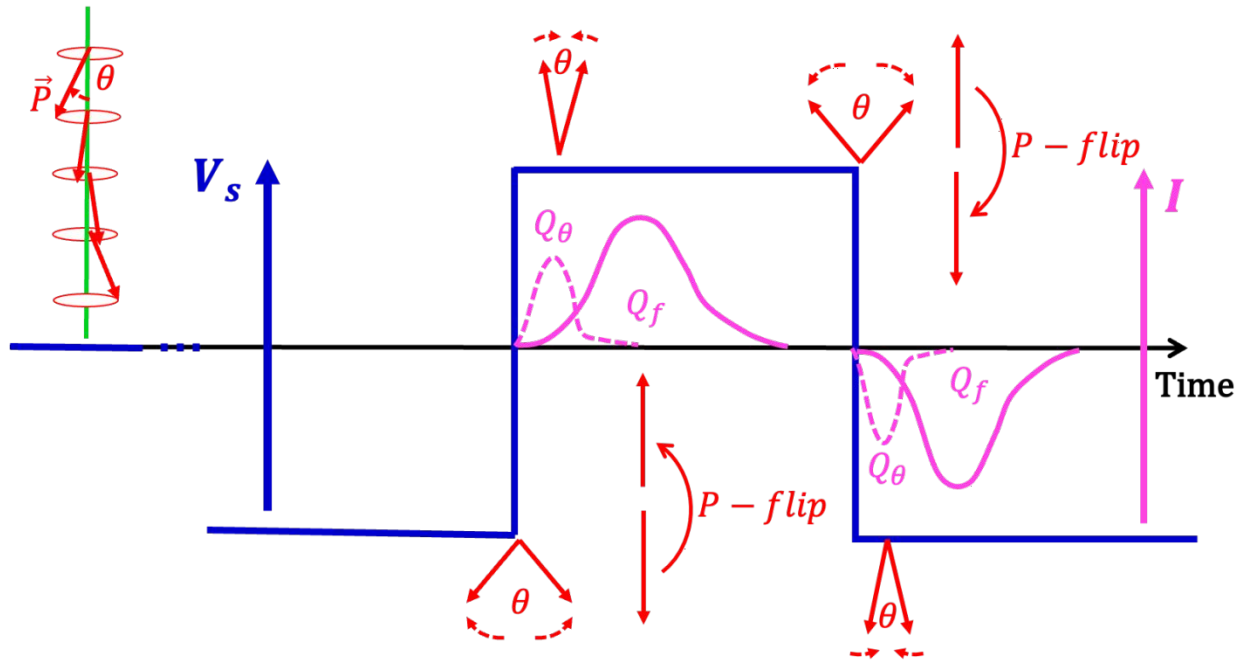


Figure 7: Schematic representation of the polarization switching mechanisms involving variation of the cone angle (θ – mode) and flipping of the polarization (P – flip) leading to two current peaks. The sketch of the director structure at zero field is shown on the left side at time before applying the square-wave voltage (blue lines). Sketch of the polarization rotation and flipping during the switching are shown with red arrows and letters below and above the time dependent voltage corresponding approximately to the time when those are happening. Pink curves and the pink vertical axis represent the time dependences of the electric current.

This means that $\cos\theta_o = \frac{Q_2}{Q_1+Q_2}$. From Figure 6(d) this gives $\theta_o \approx 34^\circ$ at $R = 5 \text{ k}\Omega$ and $\theta_o \approx 22^\circ$ at $R = 51 \text{ k}\Omega$. This may be interpreted as complete closing of the cone angle during switching at $R = 5 \text{ k}\Omega$ and only partial closing between 34° and 12° at $R = 51 \text{ k}\Omega$. We note that the estimated $\theta_o \approx 34^\circ$ at 100°C of JK103 is much larger than what was calculated by Basnet et al³¹ from birefringence data. This might be due to a pre-transitional conical structure in the N_F phase, which can be deduced from Figure 6(a) which already shows a combination of two peaks even at 110°C in the N_F phase. This indicates a non-zero pretransitional cone angle and zero-field distribution of the polarization direction. Another possible reason for the apparently larger cone-angle deduced from the switching current is the coupling between the polarization flipping and cone-angle (θ) variation. At the instant when a voltage large enough to fully switch the polarization along the field (for example under $V_s = 2.2 \text{ V}$ at $R = 5 \text{ k}\Omega$), is quickly reversed, the polarization remains in the wrong direction, which is energetically unfavorable. The faster θ -mode can reduce the free-



energy by increasing the cone angle, thus decreasing the polarization value showing in the wrong direction. As the polarization starts flipping, θ will decrease and the cone closes when all the polarization is along the field, thus further decreasing the free energy (see Figure 7). Such an interplay between the two switching modes is likely explains why for JK103 the switching time is not strictly linear function of the resistance R , as seen in Figure 6(e).

From the intercepts corresponding to the linear fit (solid lines in Figure 6(e)) we can estimate the rotational viscosities γ corresponding to the polarization flipping both in the N_F and N_{TBF} phases and of γ_θ corresponding to the θ -mode in the N_{TBF} phase. In the N_F phase at 100 °C, taking $R_{LC} = \frac{L\gamma}{AP^2} \approx 64k\Omega$ and with $L \approx 20 \mu m$, $A \approx 16 \cdot 10^4 \mu m^2$, $P \approx 4.2 \cdot \frac{10^{-2}C}{m^2}$, we estimate that $\gamma \approx 0.82 Pa \cdot s$. This larger value than we found for RM734 and DIO at similar temperatures is likely due to the longer molecule of JK103. In the N_{TBF} phase at 100 °C, $R_{LC}^f = \frac{L\gamma}{AP^2 \cos^2 \theta_o} \approx 38k\Omega$ from the linear intercept (see Figure 6(e)), which with $\theta_o \approx 34^\circ$ gives $\gamma \approx 0.34 Pa \cdot s$. This smaller value than in the higher temperature N_F phase makes sense, as now the flipping length is shorter due to the tilted polarization. From $R_{LC}^\theta = \frac{L\gamma}{AP^2(1-\cos\theta_o)^2} \approx 62k\Omega$ we get $\gamma_\theta \approx 0.14 Pa \cdot s$, which is smaller than γ as γ_θ involves smaller rotation of the director.

V. Conclusions

In this work we have described negative capacitance (NC) of two prototypical ferroelectric nematic liquid crystals RM734 and DIO. The presented results and additional studies on a number of other ferroelectric nematic liquid crystals in their N_F phase strongly suggest that all N_F materials show NC provided that the polarization switching time is larger than of the rise time of the applied square-wave voltage.

Additionally, we have observed NC in one of the recently discovered fluid twist-bend ferroelectric nematic liquid crystal (N_{TBF}) materials JK103 while electrically switching their ferroelectric polarization. In contrast to 2 NC ranges found in conventional solid and fluid ferroelectric materials, in the N_{TBF} phase the polarization switching happens in two steps leading to four negative capacitance ranges in the P-V hysteresis curves. Our measurements and analyses also provided estimates of the rotational viscosities related to the flipping of the polarization ($P - flip$) and to the variation of the heliconical angle ($\theta - mode$). Based on these results, we also



provided models for these two switching mechanisms and explained similarities and differences between our and previous models.

VI. Acknowledgement

This work was financially supported by the US National Science Foundation grant DMR-2210083 and the Hungarian NKFIH FK142643.

VII. References

- 1 L. D. Landau and I. M. Khalatnikov, *Dokl. Akad. Nauk.*, 1954, **96**, 469–472.
- 2 J. Íñiguez, P. Zubko, I. Luk'yanchuk and A. Cano, *Nat. Rev. Mater.*, 2019, **4**, 243–256.
- 3 A. M. Bratkovsky and A. P. Levanyuk, *Appl. Phys. Lett.*, DOI:10.1063/1.2408650.
- 4 P. Chandra and Littlewood P. B., in *Physics of Ferroelectrics: A Modern Perspective*, 2007, pp. 69–116.
- 5 M. Hoffmann, A. I. Khan, C. Serrao, Z. Lu, S. Salahuddin, M. Pešić, S. Slesazeck, U. Schroeder and T. Mikolajick, *J. Appl. Phys.*, 2018, **123**, 184101–10.
- 6 M. Hoffmann, S. Slesazeck and T. Mikolajick, *APL Mater.*, 2021, **9**, 020902–1.
- 7 M. Hoffmann, P. V. Ravindran and A. I. Khan, *Materials*, 2019, **12**, 3743.
- 8 A. I. Khan, K. Chatterjee, B. Wang, S. Drapcho, L. You, C. Serrao, S. R. Bakaul, R. Ramesh and S. Salahuddin, *Nat. Mater.*, 2015, **14**, 182–186.
- 9 A. K. Yadav, K. X. Nguyen, Z. Hong, P. García-Fernández, P. Aguado-Puente, C. T. Nelson, S. Das, B. Prasad, D. Kwon, S. Cheema, A. I. Khan, C. Hu, J. Íñiguez, J. Junquera, L. Q. Chen, D. A. Muller, R. Ramesh and S. Salahuddin, *Nature*, 2019, **565**, 468–471.
- 10 M. Hoffmann, F. P. G. Fengler, M. Herzig, T. Mittmann, B. Max, U. Schroeder, R. Negrea, L. Pintilie, S. Slesazeck and T. Mikolajick, *Nature*, 2019, **565**, 464–467.
- 11 J. Doherty, K. A. Lynch and I. Ponomareva, *J. Appl. Phys.*, 2022, **132**, 034101.



- 12 M. Hoffmann, Z. Wang, N. Tasneem, A. Zubair, P. V. Ravindran, M. Tian, A. A. Gaskell, D. Triyoso, S. Consiglio, K. Tapily, R. Clark, J. Hur, S. S. K. Pentapati, S. K. Lim, M. Dopita, S. Yu, W. Chern, J. Kacher, S. E. Reyes-Lillo, D. Antoniadis, J. Ravichandran, S. Slesazeck, T. Mikolajick and A. I. Khan, *Nat. Commun.*, 2022, **13**, 1228.
- 13 N. P. Dhakal, A. Adaka, R. J. Twieg, N. A. Clark and A. Jákli, *Phys. Rev. Appl.*, DOI:10.1103/fjx3-jd2y.
- 14 X. Chen, E. Korblova, D. Dong, X. Wei, R. Shao, L. Radzihovsky, M. A. Glaser, J. E. MacLennan, D. Bedrov, D. M. Walba, N. A. Clark, N. L. Abbott, P. Palfy-Muhoray, P. Pieranski, N. A. C. Designed and N. A. C. Performed, *PNAS*, 2020, **117**, 14021–14031.
- 15 N. Sebastián, M. Čopič and A. Mertelj, *Phys. Rev. E*, 2022, **106**, 021001–1.
- 16 H. Nishikawa, K. Shiroshita, H. Higuchi, Y. Okumura, Y. Haseba, S. I. Yamamoto, K. Sago and H. Kikuchi, *Advanced Materials*, 2017, **29**, 1702354.
- 17 P. Guragain, A. Ghimire, M. Badu, N. P. Dhakal, P. Nepal, J. T. Gleeson, S. Sprunt, R. J. Twieg and A. Jákli, *Mater. Horiz.*, 2025, **12**, 8153–8164.
- 18 B. Basnet, M. Rajabi, H. Wang, P. Kumari, K. Thapa, S. Paul, M. O. Lavrentovich and O. D. Lavrentovich, *Nat. Commun.*, 2022, **13**, 3932.
- 19 X. Chen, E. Korblova, M. A. Glaser, J. E. MacLennan, D. M. Walba and N. A. Clark, *PNAS*, 2021, **118**, e2104092118.
- 20 N. Vaupotič, T. Krajnc, E. Gorecka, D. Pocięcha and V. Matko, *Liq. Cryst.*, DOI:10.1080/02678292.2025.2484234.
- 21 M. A. Osipov, *Liq. Cryst.*, DOI:10.1080/02678292.2025.2528729.
- 22 V. Matko, E. Gorecka, D. Pocięcha, J. Matraszek and N. Vaupotič, *Phys. Rev. Res.*, 2024, **6**, L042017.
- 23 N. A. Clark, X. Chen, J. E. MacLennan and M. A. Glaser, *Phys. Rev. Res.*, 2024, **6**, 013195.
- 24 A. Adaka, M. Rajabi, N. Haputhantrige, S. Sprunt, O. D. Lavrentovich and A. Jákli, *Phys. Rev. Lett.*, 2024, **133**, 038101.



- 25 A. Paul, M. Paul, M. Badu, A. Ghimire, N. P. Dhakal, S. Sprunt, A. Jákli and J. T. Gleeson, *Materials*, 2025, **18**, 5496–5509.
- 26 H. Nishikawa, P. Salamon, M. T. Máthé, A. Jákli and F. Araoka, *Giant*, 2025, **22**, 100356.
- 27 R. J. Mandle, S. J. Cowling and J. W. Goodby, *Physical Chemistry Chemical Physics*, 2017, **19**, 11429–11435.
- 28 J. Karcz, J. Herman, N. Rychłowicz, P. Kula, E. Górecka, J. Szydłowska, P. W. Majewski and D. Pocięcha, *Science (1979)*, 2024, **384**, 1096–1099.
- 29 P. Kumari, B. Basnet, M. O. Lavrentovich and O. D. Lavrentovich, *Science (1979)*, 2024, **383**, 1364–1368.
- 30 A. B. Szukalska, J. Karcz, J. Herman, D. Pocięcha, E. Górecka, P. Kula and J. Myśliwiec, *Advanced Materials*, 2026, **38**, e11648.
- 31 B. Basnet, P. Kumari, S. Paladugu, D. Pocięcha, J. Karcz, P. Kula, N. Vaupotič, E. Górecka and O. D. Lavrentovich, *Advanced Science*, 2025, e15752.
- 32 H. Nishikawa, D. Okada, D. Kwaria, A. Nihonyanagi, M. Kuwayama, M. Hoshino and F. Araoka, *Advanced Science*, 2024, **11**, 2405718.
- 33 D. Chen, J. H. Porada, J. B. Hooper, A. Klittnick, Y. Shen, M. R. Tuchband, E. Korbloèa, D. Bedrov, D. M. Walba, M. A. Glaser, J. E. MacLennan and N. A. Clark, *Proc. Natl. Acad. Sci. U. S. A.*, 2013, **110**, 15931–15936.
- 34 V. Borshch, Y.-K. Kim, J. Xiang, M. Gao, A. Jakli, V. P. Panov, J. K. Vij, C. T. Imrie, M. G. Tamba, G. H. Mehl and O. D. Lavrentovich, *Nat. Commun.*, 2013, **4**, 2635-1–8.
- 35 G. J. Strachan, E. Górecka and D. Pocięcha, *Mater. Horiz.*, 2026, **13**, 779.
- 36 G. J. Strachan, E. Górecka, J. Hobbs and D. Pocięcha, *J. Am. Chem. Soc.*, 2025, **147**, 6058–6066.
- 37 J. Hobbs, C. J. Gibb and R. J. Mandle, *Nature Communications*, 2025, **16**, 7510.
- 38 H. Nishikawa, K. Shiroshita, H. Higuchi, Y. Okumura, Y. Haseba, S. I. Yamamoto, K. Sago and H. Kikuchi, *Advanced Materials*, 2017, **29**, 1702354–1702354.



- 39 X. Chen, E. Korblova, D. Dong, X. Wei, R. Shao, L. Radzihovsky, M. A. Glaser, J. E. Maclennan, D. Bedrov, D. M. Walba and N. A. Clark, *Proc Natl Acad Sci USA*, 2020, **117**, 14021–14031.
- 40 H. Nishikawa, D. Kwaria, A. Nihonyanagi and F. Araoka, *Advanced Materials*, 2025, **38**, e13451.
- 41 C. J. Gibb, J. Hobbs, D. I. Nikolova, T. Raistrick, S. R. Berrow, A. Mertelj, N. Osterman, N. Sebastián, H. F. Gleeson and R. J. Mandle, *Nat. Commun.*, 2024, **15**, 5845.



Data Availability Statement

The data supporting this study are available from the corresponding author upon reasonable request.

